Environmental Engineering of Pd Nanoparticle Catalysts for Catalytic Hydrogenation of CO_2 and Bicarbonate

*Li-Chen Lee, Xiaoyu Xing, and Yan Zhao**

Department of Chemistry, Iowa State University, Ames, Iowa 50011-3111

zhaoy@iastate.edu

ABSTRACT. The extraordinary catalytic properties of enzymes are derived not only from their catalytic groups but also the unique properties of the active site. Tuning the microenvironment of synthetic catalysts is expected to enhance their performance if effective strategies can be developed. Interfacially cross-linked reverse micelles were prepared from three different cross-linkable surfactants. Pd nanoparticles were deposited in the core of the micelle for the catalytic hydrogenation of bicarbonate and CO_2. The catalytic performance was found to depend heavily on the nature of the headgroup of the surfactant. Quaternary ammonium-based surfactants through ion exchange could bring bicarbonate to the catalytic center, whereas tertiary amine-based surfactants worked particularly well in CO_2 hydrogenation, with turnover numbers an order of magnitude higher than that of commercially available Pd/C. The amines were proposed to bring CO_2 to the proximity of the catalysts through reversible formation of carbamate, in the nanospace of the hydrophilic core of the cross-linked reverse micelle. In the bicarbonate reduction, additional improvement of the catalysts was achieved through localized sol–gel synthesis that introduced metal oxide near the catalytic metal.

Keywords: nanoparticle, catalysis, cross-linking, reverse micelle, hydrogenation

Introduction

Instead of solely relying on catalytic metals and ligands in their first coordination sphere, enzymes frequently employ ligands at the second coordination sphere and even remote allosteric binding sites to enhance catalytic activity and selectivity. In the last decades, tremendous progress has been made by chemists in the design and synthesis of organometallic, organic, and metal particle catalysts. More recently, there is increasing recognition for the importance of second-sphere or more distal control in catalysis.[1,2] Various platforms such as dendrimers,[3-5] star polymers,[6,7] organic and metal-organic nanocapsules,[8-11] multifunctional mesoporous materials,[12-15] and metal-organic frameworks[16-19] have been used to tune the catalytic properties of attached or encapsulated catalysts. Toward this effort, our group reported amphiphilic baskets,[20] foldamers,[21] and surface-cross-linked micelles[22-24] for similar purposes.

Despite the advancement made by different researchers, much remains to be learned in the "microenvironmental engineering" of a catalyst for improved performance. Because the environment around the catalyst is larger than the catalyst, construction of a tailored, multifunctional microenvironment could require even more synthetic effort than the synthesis of the catalyst itself—such is indeed the case for enzymes whose active site is but a portion of the entire structure.

Reverse micelles (RMs) are dynamic aggregates of surfactants formed in nonpolar solvents with a nanosized water pool in the center.[25,26] Once captured by covalent bonds, they become interesting organic nanoparticles with a hydrophilic core and hydrophobic exterior.[27,28] Our group reported that polymerization/cross-linking at the surfactant/water interface was particularly effective at capturing RMs in nearly the original size (4–5 nm).[29] When conventional RMs are used as templates to prepare inorganic nanoparticles, their diffusion-controlled collision and exchange of internal contents make it difficult to control the size and morphology of the final materials.[30,31] Our interfacially cross-linked reverse micelles (ICRMs), due to their covalent nature, made the templated synthesis of metal nanomaterials facile and highly predictable. The same template allowed us to prepare metal clusters consisting of a few atoms and nanoparticles several nanometers in size, by controlling the amount of metal loading and reduction method.[32]

Hydrogenation of CO_2 has been under intense investigation for many decades.[33-39] Because the formic acid from CO_2 hydrogenation can be dehydrogenated under mild conditions to release CO_2, the reaction couple could be used as a potential hydrogen storage material as well.[34,35,39] Among the heterogeneous catalysts, Pd/C was one of the first catalysts reported to catalyze hydrogenation of bicarbonate to formate in aqueous solution.[40,41] In recent years, researchers continue to improve Pd-catalyzed hydrogenation of bicarbonate or CO_2, using different bicarbonate salts, alloys, or catalytic supports.[42-45] Remarkable progress in catalytic efficiency has been achieved in some systems.[46,47]

In this work, we report that Pd-containing ICRMs could be used to hydrogenate bicarbonate and CO_2 to formate. The model reaction was chosen to demonstrate the strategy of modeulating catalysis through rational environmental engineering of the catalysts. Our Pd@ICRM catalysts showed turnover numbers (TONs) an order of magnitude higher than that displayed by commercially available Pd/C catalysts for CO_2 hydrogenation. Most interestingly, the microenvironment of the Pd nanoparticles could be controlled by the surfactant headgroups of the ICRMs so that the catalysts could be made to favor bicarbonate or CO_2. For bicarbonate reduction, tiny amounts of metal oxides could be deposited on the Pd nanoparticle through confined sol–gel synthesis to further improve the catalytic properties.

Results and Discussion

Design and Syntheses of Pd@ICRMs. As shown by Scheme 1, we used three triple-tailed cross-linkable surfactants (**1**–**3**) in the synthesis of the ICRMs. Compounds **1** and **3** are quaternary ammonium salts and **2** is a protonated amine. The wedge-shaped surfactants have a large hydrophobic volume in comparison to the polar headgroup, making it easy for them to pack in the RM configuration.[48] Surfactant **1** has three allyl groups and was cross-linked at the interface using a hydrophilic dithiol (dithiothreitol or DTT) under UV irradiation.[29] Surfactants **2** and **3** both have two polymerizable methacrylamides and could be cross-linked directly by photo-induced free radical polymerization.[49] Although the methacrylamide and the amine/ammonium center in **2** and **3** has different number of methylene groups in

between, the difference was minor and was due to different commercially available starting materials used in the synthesis.

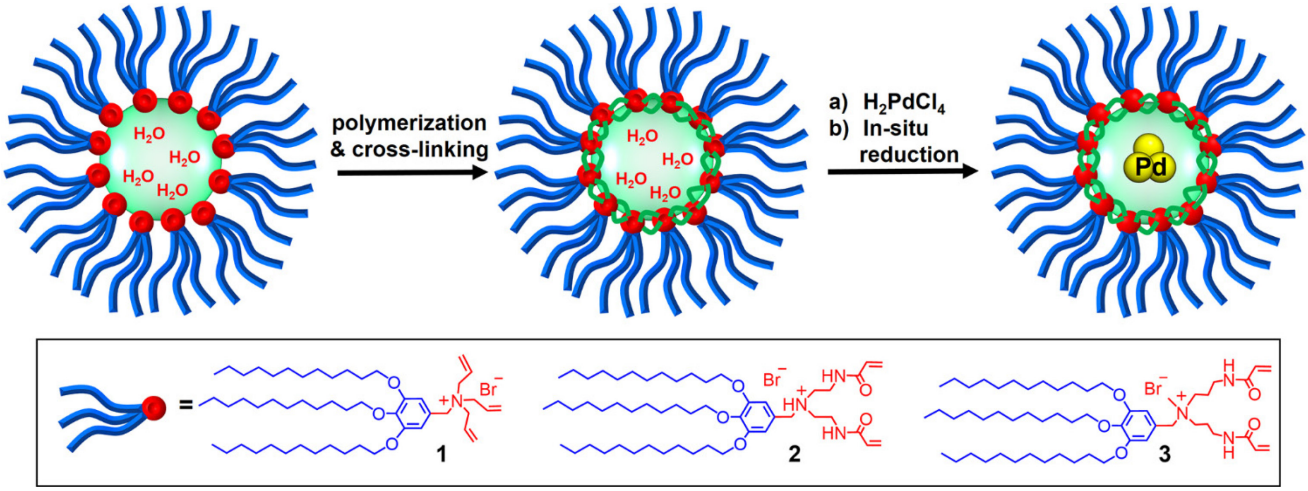

Scheme 1. Preparation of Pd@ICRM from cross-linkable surfactants **1**–**3**.

Detailed procedures for the preparation of ICRMs have been reported previously.[29,49] In general, RMs were first formed by dissolving an appropriate surfactant in heptane, with a tiny amount of water. Polymerization and cross-linking of the RMs were induced by a hydrophilic photoinitiator, 2-hydroxy-1-(4-(2-hydroxyethoxy)phenyl)-2-methylpropan-1-one, under UV irradiation.[49] The reaction was typically complete within 2 h and the ICRMs were obtained after evaporation of the solvent and washing with cold methanol.

With numerous cationic groups in the core, the ICRMs could extract anionic salts such as H_2PdCl_4 from an aqueous solution. The palladium salts were reduced in situ during hydrogenation to afford nanoparticles in the core. The ICRM[29,49] and Pd@ICRM[50] were characterized using ^{1}H NMR spectroscopy, dynamic light scattering (DLS), UV-vis spectroscopy, and transmission electron microscopy (TEM). In general, the size of the ICRM was 4–5 nm and the Pd nanoparticles inside ~2 nm. For the optimized catalyst identified in this study, Pd/Al_2O_3@ICRM(**3**), additional STEM and EDX elemental mapping were also performed (Figure 1). In addition to providing information on the size of the ICRMs, the characterizations showed that intimate mixing of palladium and aluminum on the nanoscale, consistent with our ICRM-template sol–gel synthesis (vide infra).

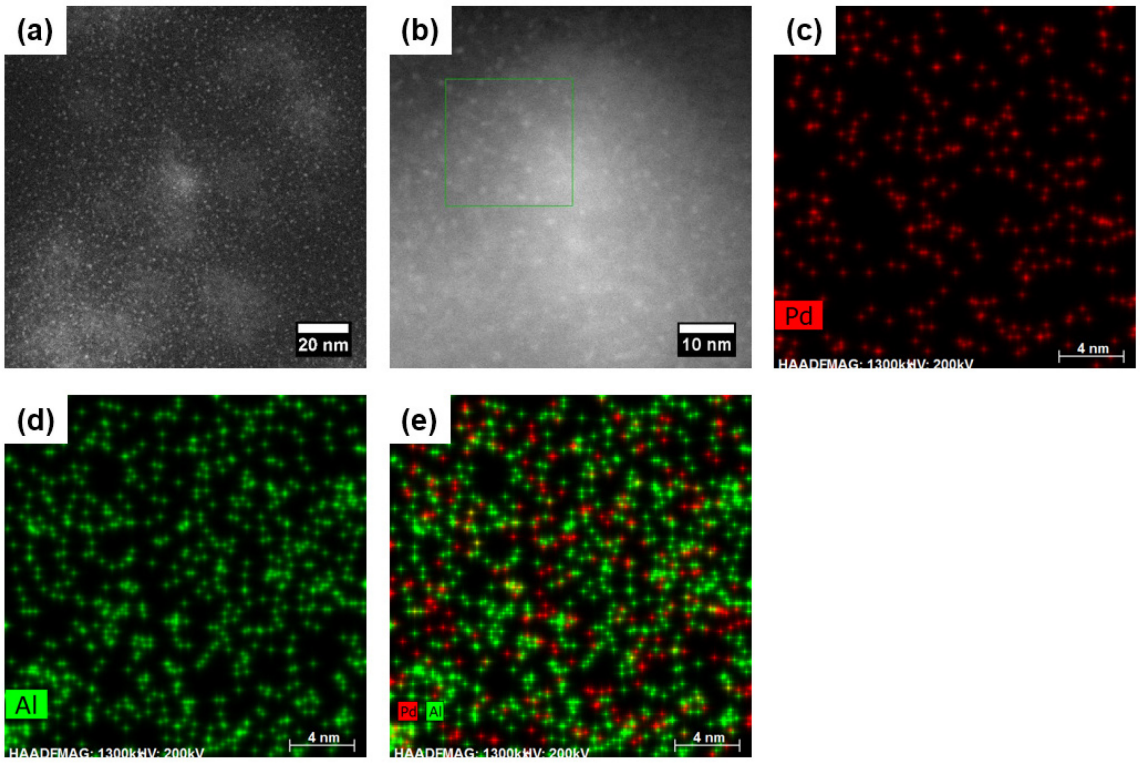

Figure 1. (a) HAADF-STEM image of Pd@ICRM(**3**). The ICRMs were imaged in dark field and shown as bright spots in the image. (b) HAADF-STEM image of Pd/Al_2O_3@ICRM(**3**) and EDX elemental mapping of the selected area (rectangle indicated by green solid line in b) for Pd (c), Al (d), and Pd and Al overlay (e). In the STEM images, The Pd@ICRM was prepared from surfactant **3** with Pd-loading = $[H_2PdCl_4]$/[**3**] = 50% and $W_0 = 20$.

The structure of the ICRM allows us to engineer the microenvironment of the Pd nanoparticles in a rational manner. For Pd@ICRM(**1**) and Pd@ICRM(**3**), the quaternary ammonium groups in the core make is possible to exchange the bromide with other anions including tetrachloroaurate, nitrate, chloride, and azide.[29,32,50-52] These catalysts should work well for the hydrogenation of bicarbonate, as ion exchange would bring the substrate to the ICRM core, where the Pd catalysts reside (Scheme 2, up panel). On the other hand, Pd@ICRM(**3**) should work particularly well for CO_2 hydrogenation (Scheme 2, lower panel). Organic amines are frequently used to capture gaseous CO_2 reversibly through carbamate formation.[53] Although **2** was used as the HBr salt during the ICRM preparation—which is necessary for the RM formation—the large quantities of amine (0.7 M Et_3N) used in the hydrogenation (vide infra) should

readily deprotonate the tertiary amine–HBr salts in the ICRM core. Because numerous amine groups are present in Pd@ICRM(**3**), plenty of them should be in the free form (instead of complexing with the entrapped Pd nanoparticles). These amines are expected to form carbamate with CO_2 and, as a result, bring the reactant to the Pd catalysts located in the nanosized ICRM core. Since there is significant distance in the surfactants between the cross-linkable groups, the cross-linking should not impede the diffusion of small reactants such as CO_2 and H_2 into the catalytic metals inside the ICRM core. The facile ion-exchange of the anions in the ICRMs also supported the notion.[29,32,50-52]

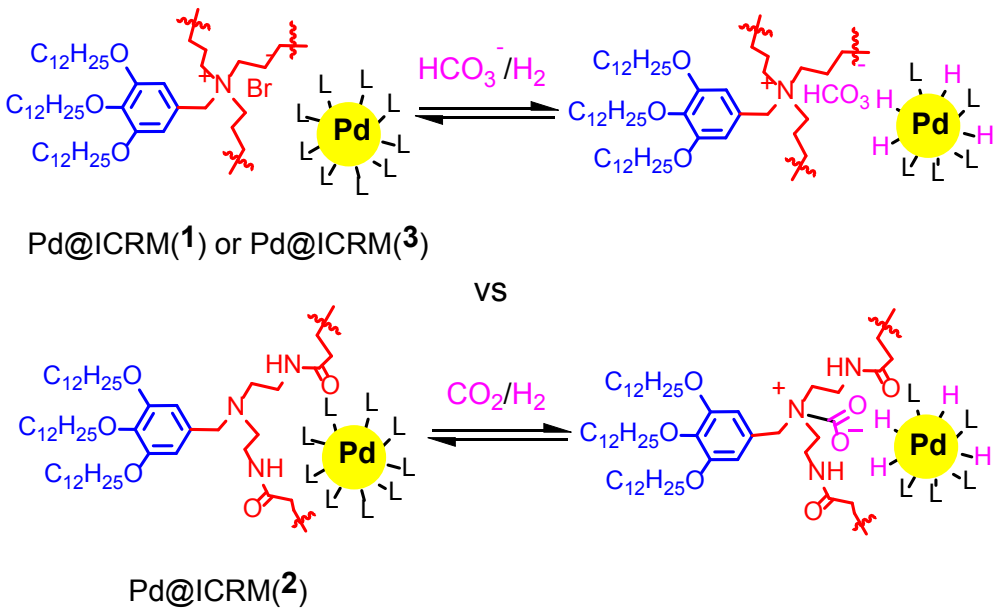

Scheme 2. Microenvironmental engineering of Pd nanoparticle catalysts for the hydrogenation of bicarbonate and CO_2.

Hydrogenation of Bicarbonate by Pd@ICRMs. Many homogeneous catalysts have been reported to convert CO_2 to formic acid or formate, some with extraordinary activities.[54-63] Heterogeneous catalysts have some distinctive advantages over homogeneous ones but generally showed lower activity.[42,43] Among the heterogeneous catalysts, Pd/C was one of the first catalysts used to catalyze hydrogenation of bicarbonate.[40,41] Although Pd metal clearly was active in the reaction, commercially available catalysts have relatively low turnover numbers (TONs) in the range of 20 to 115 at 0.3–1.0 M $NaHCO_3$ in the aqueous phase.[40]

Table 1 shows the hydrogenation of sodium bicarbonate in a 2:3 THF/water mixture under different conditions. It is known that the equilibrium between CO_2 and bicarbonate is influenced by many parameters and there is thus some ambiguity of the nature of the exact reactant.[42] In this work, we classified our reactions based on the initial starting materials used. Reaction yields were determined by ^{1}H NMR spectroscopy with DMF as the internal standard. The reaction was clean, with no other products observed (Figure 3S in the Supporting Information). No product was observed without Pd-loading in the ICRMs. The catalysts prepared from **1** as the cross-linkable surfactant were completely inactive but similar catalysts prepared from **2** gave good yields up to 82% (entry 4). It is possible the sulfide in the ICRM core derived from DTT (the cross-linking agent) poisoned the metal in Pd@ICRM(**1**). We have seen similar results when the ICRM prepared from similar DTT cross-linking contained gold catalysts.[49]

Table 1. Hydrogenation of sodium bicarbonate by Pd@ICRM.[a]

Entry	surfactant	W_0	Pd-loading	T (°C)	% yield[b]	TON
1	**1**	20	10%	80[c]	trace	0
2	**1**	20	50%	80[c]	trace	0
3	**2**	20	10%	80[c]	32	32
4	**2**	20	50%	80[c]	82	82
5	**2**	20	50%	40[c]	100	100
6	**2**	20	50%	rt[c]	17	17
7	**2**	5	50%	rt[d]	7	7
8	**2**	10	50%	rt[d]	8	8
9	**2**	20	50%	rt[d]	10	10
10	**3**	5	50%	rt[d]	33	33
11	**3**	10	50%	rt[d]	39	39
12	**3**	20	50%	rt[d]	48	48
13	**3**	20	10%	rt[d]	13	13
14	**3**	20	30%	rt[d]	25	25
15	**3**	20	80%	rt[d]	36	36
16	**3**	20	100%	rt[d]	38	38

[a] W_0 was the water/surfactant ratio during the ICRM preparation. Pd-loading = [H_2PdCl_4]/[cross-linkable surfactant]. Because the Pd@ICRM catalysts are soluble in common organic solvents, no recycling of catalysts was performed in the current study. [b] The percent yield was determined by ^{1}H-NMR spectroscopy with 0.1 mmol DMF as the internal standard based on the conversion of bicarbonate. [c] The reaction was carried out in 0.2 mL THF and 0.3 mL D_2O under 40 bar CO_2 and 40 bar H_2 for 20 h with 0.1 mmol $NaHCO_3$ and 0.001 mmol Pd. [d] The reaction was carried out in 0.2 mL THF and 0.3 mL D_2O under 40 bar H_2 for 8 h with 0.1 mmol $NaHCO_3$ and 0.001 mmol Pd. No product was observed without Pd-loading in the ICRMs.

The amount of palladium in the ICRM core made a big difference, as lower Pd-loading in the core gave a lower yield in the hydrogenation even when the total amount of Pd in the reaction was kept at 1 mol % (entries 3 and 4). With the same Pd@ICRM(**2**) catalysts, the yield of formate was higher at 40 °C than at either 80 °C or room temperature (entries 4–6).

These initial screenings were performed under 40 bar CO_2 and 40 bar H_2 for 20 h (entries 1–6). CO_2 was added in the gas phase because of the low activity of the catalysts. Once reasonable catalysts were identified, we left CO_2 out in the gas phase and performed the reaction at room temperature for a shorter period of time of 8 h (entries 7–16). The conversion yield was expectedly lower (compare entries 6 and 9). The yield was also somewhat lower at 80 °C than at 40 °C (entries 4 and 5). This probably reflected the fact that hydrogenation of bicarbonate is entropically unfavorable because a gaseous reactant is converted to formate in the solution.

Our data show that the water/surfactant ratio (W_0), which controls the size of the hydrophilic core of the ICRM,[29] also influenced the catalysis. In general, a larger hydrophilic core was better (entries 7–12). Since our surfactants have limited abilities to include water in the RM core, we limited water/surfactant ratio to ≤20.[29]

We also varied the Pd-loading (i.e., the [H_2PdCl_4]/[cross-linkable surfactant] ratio) in the ICRM(**3**) from 10 to 100%, and found that 50% gave the best results (entries 12–16). The initial increase and then

decrease of TON with Pd-loading seems to make sense. If the mechanism in Scheme 2 is operating, the Pd/ammonium ratio is expected to be important to the catalysis. If too little Pd is present, even if the ammonium groups on the surfactants could bring bicarbonate into the ICRM core, the bicarbonate might not have a nearby catalytic Pd particle for the subsequent hydrogenation. If too much Pd is present, there could be very little room left in the core to accommodate the bicarbonate ions. It is also possible that the size of the Pd nanoparticles also played a role. Our previous work showed that the size of the metal particles obtained from ICRM-templated synthesis generally increased with the metal loading in the ICRM.[29] Since the best results were obtained with 50% loading in Table 1, there is no simple correlation between the size and the catalytic activity.

The results so far indicate that the ICRM is playing an important role in the Pd-catalyzed bicarbonate reduction. The quaternary ammonium-based Pd@ICRM from **3** was significantly more reactive than the tertiary amine-based catalysts from **2**, consistent with the ion-exchange model.[29,32,50-52] Nonetheless, the catalysts at this point were still rather inefficient.

Metal particles in heterogeneous catalysis are known to be strongly influenced by their metal oxide support.[5,64-67] Because RMs are frequently used as templates for metal oxides,[25] we could incorporate metal oxides in the ICRM core. This is an important feature of the ICRM framework to further engineer the microenvironment of the catalysts.

To introduce metal oxides to the ICRM core, we typically first dissolve Pd@ICRM in a chloroform solution. We then add a small amount of water (typically 5 equiv to the cross-linked surfactant) and a hydrolysable metal precursor— $Si(OMe)_4$ for SiO_2, $SnCl_4$ for SnO_2, $Ti(OiPr)_4$ for TiO_2,and (s-BuO)$_3$Al for Al_2O_3.[52,68] Because water prefers to stay near the hydrophilic ICRM core in a chloroform solution, hydrolysis of the metal precursor occurs near the ICRM core, in the proximity of the Pd metal. The process is essentially a miniature sol–gel hydrolysis localized near the water "puddle" in the center of the ICRM. We typically allowed the hydrolysis to proceed for 24 h (48 h for SiO_2) until ^{1}H NMR spectroscopy shows the completion of the reaction (by the release of the alcohol product).[52,68] Throughout the process, the

solution stays clear. In the absence of the ICRM, the same sol–gel hydrolysis yields precipitates quickly from the chloroform solution.

Encouragingly, the localized metal oxides—or most likely their hydrates due to the low temperature involved—strongly impacted the catalysis (Table 2). Whereas SiO_2 inhibited the catalysis, the other three metal oxides improved the conversion to different degrees (entries 1–5). Among the metal oxides examined, Al_2O_3 was the clear winner, affording a 96% yield at 40 bar H_2 at room temperature. When the amount of Pd was reduced to 0.1 mol%, the TON increased to 320 (entry 8). Importantly, the intimate contact between Pd and the metal oxide was critical to the improved catalysis, as Pd@ICRM(**3**) and Al_2O_3@ICRM mixed in the same solution gave slightly worse results than Pd@ICRM(**3**) (compare entries 1 and 10). As expected, Al_2O_3@ICRM(**3**) without Pd in the core showed no activity (entry 9).

Table 2. Hydrogenation of sodium bicarbonate by Pd@ICRM(**3**) prepared with local metal oxides.[a]

Entry	metal oxide	mol % Pd	% yield[b]	TON
1	none	1.0	48	48
2	SiO_2	1.0	15	15
3	SnO_2	1.0	67	67
4	TiO_2	1.0	88	88
5	Al_2O_3	1.0	96	96
6	Al_2O_3	0.7	67	96
7	Al_2O_3	0.4	52	130
8	Al_2O_3	0.1	32	320
9	Al_2O_3	0	0	0
10	Al_2O_3	1.0	43[c]	43

[a] The ICRM was prepared from surfactant **3** with Pd-loading = $[H_2PdCl_4]/[\mathbf{3}]$ = 50% and W_0 = 20. The reaction was carried out in 0.2 mL THF and 0.3 mL D_2O at room temperature under 40 bar H_2 for 8 h with 0.1 mmol $NaHCO_3$. [b] The percent yield was determined by ^{1}H-NMR spectroscopy with 0.1 mmol DMF as the internal standard based on the conversion of bicarbonate. [c] The reaction was catalyzed by Pd@ICRM and Al_2O_3@ICRM and thus the Pd metal and Al_2O_3 were in different ICRMs.

It is unclear to us at this point why Al_2O_3 gave the best results in bicarbonate hydrogenation. In the literature, Al_2O_3 was not the best support for Pd-catalyzed hydrogenation of ammonium bicarbonate.[43] In the hydrogenation of CO_2 by Pd@ICRM, the localized Al_2O_3 actually lowed the reaction yield (vide infra). Thus, the metal oxide did not bring a general enhancement of the catalytic activity. Since ion exchange is critical to taking the reactant to the catalyst in the bicarbonate reduction, we suspect the metal oxide might have helped the ion exchange process.

Solvent effects can be greatly magnified in a nanospace due to significant size of the solvent relative to the environment.[69,70] The bicarbonate hydrogenation also showed a strong dependency on the solvents (Table 3). Among the solvents tried, the biphasic chloroform/water mixture probably slowed down the mass transfer dramatically, as the ICRM and substrate (bicarbonate) were located in two immiscible solvents. DMSO also suppressed the reactivity completely. It is not exactly clear why methanol gave a much lower yield than THF and 1,4-dioxane. We suspect that the hydrogen-bonding-capable alcohol can solvate bicarbonate better than ether, and may have inhibited the ion exchange by stabilizing them in the bulk solvents. As discussed earlier, the very different behavior between Pd@ICRMs made from **2** and **3** suggests ion exchange was an important factor in the hydrogenation. Finally, inclusion of CO_2 in the gas phase expectedly enhanced the TON further, up to 830 with 40 bar of the gas.

Table 3. Hydrogenation of sodium bicarbonate by 0.1 mol % of Pd/Al_2O_3@ICRM(**3**) under different conditions.[a]

Entry	solvent	CO_2 in the gas phase	% yield[b]	TON
1	THF/D_2O = 2:3	0 bar	32	320
2	MeOH/D_2O = 2:3	0 bar	11	110
3	DMSO/D_2O = 2:3	0 bar	0	0
4	$CHCl_3$/D_2O = 2:3	0 bar	0	0
5	D_2O	0 bar	7	70
6	1,4-dioxane/D_2O = 1:4	0 bar	34	340

7	1,4-dioxane/D_2O = 2:3	0 bar	48	480
8	1,4-dioxane/D_2O = 3:2	0 bar	58	580
9	1,4-dioxane/D_2O = 4:1	0 bar	28	280
10	1,4-dioxane/D_2O = 3:2	20 bar	82	820
11	1,4-dioxane/D_2O = 3:2	40 bar	83	830

[a] The ICRM was prepared from surfactant **3** with Pd-loading = [H_2PdCl_4]/[**3**] = 50% and W_0 = 20. The reaction was carried out in 0.2 mL THF and 0.3 mL D_2O under 40 bar H_2 at room temperature for 8 h with 0.1 mmol $NaHCO_3$ and 0.0001 mol Pd [b] The percent yield was determined by ^{1}H-NMR spectroscopy with 0.1 mmol DMF as the internal standard based on the conversion of bicarbonate.

Hydrogenation of CO_2 by Pd@ICRMs. Ion exchange thus seemed to be quite helpful to the catalytic activity of Pd@ICRM(**3**). Having the substrate and the catalysts in the nanospace of the ICRM core was probably quite important to the enhanced activity. If indeed the improved catalysis was caused by the microenvironmental effect of the ICRM, we expect Pd@ICRM(**2**) to work better than Pd@ICRM(**3**) for the hydrogenation of CO_2, based on the carbamate mechanism shown in Scheme 2.

Table 4 shows the hydrogenation of CO_2 in a 2:3 THF/water mixture under different conditions. As in reported literature,[34] we performed the reaction with a relatively high concentration of base (0.7 M Et_3N) to increase the thermodynamic driving force of the reaction.

As in the bicarbonate reduction, we varied the amount of Pd-loading for the CO_2 reduction. Our study shows that, once again, 50% Pd-loading in the ICRM core gave the best results (Table 4, entries 1–5). Note that the overall amount of Pd (0.001 mmol) was kept constant for all the reactions. The water/surfactant ratio (W_0), which controls the size of the hydrophilic core, also had some impact. At constant Pd-loading (50%), TON was significantly higher at W_0 = 20 and 10 (entries 3 and 6) than at W_0 = 5 (entry 7).

Table 4. Hydrogenation of CO_2 by Pd@ICRM.[a]

Entry	catalyst	Pd-loading[b]	W_0	TON

1	Pd@ICRM(**2**)	10%	20	50
2	Pd@ICRM(**2**)	30%	20	61
3	Pd@ICRM(**2**)	50%	20	204
4	Pd@ICRM(**2**)	80%	20	91
5	Pd@ICRM(**2**)	100%	20	73
6	Pd@ICRM(**2**)	50%	10	204
7	Pd@ICRM(**2**)	50%	5	57
8	Pd@ICRM(**3**)	50%	20	69
9	Pd@ICRM(**3**)	50%	10	54
10	Pd@ICRM(**3**)	50%	5	46
11	Pd/C	50%	10	14
12	$PdCl_2$	50%	20	10

[a] The reaction was performed in 0.2 mL THF and 0.3 mL D_2O under 40 bar H_2 and 40 bar CO_2 at 40 °C for 20 h with 0.001 mmol Pd and 0.350 mmol Et_3N. The amount of formate formed was determined by ^{1}H-NMR spectroscopy with 0.1 mmol DMF as the internal standard. [b] Pd-loading = $[H_2PdCl_4]$/[cross-linkable surfactant] during the catalyst preparation.

These are promising results. In the literature, (heterogeneous) Pd metal catalysts generally were only used to reduce bicarbonate.[40-43] Direct hydrogenation of CO_2 using Pd/Ni alloy on a carbon nanotube-graphene support had a TON of 6.4,[44] with the catalytic activity improved by a graphitic carbon nitride support.[45]

It is important that the functional groups and the structures of ICRM had a strong influence over the catalysis. The positive correlation between W_0 and the catalysis agreed with literature reports that small amounts of water are beneficial to CO_2 hydrogenation when the reaction was performed in organic solvents.[34] Consistent with the importance of the localized amino groups in the ICRM core, Pd@ICRM(**3**) exhibited significantly lower activity, with TON ranging from 46–69 under similar conditions (Table 4, entries 8–10). Commercially available Pd catalysts including Pd/C and $PdCl_2$ had a much lower TON number (<15, entries 11–12).

Since the reaction mixture contains 0.7 M Et_3N, a generic effect of amine could not explain the different activities of Pd@ICRM(**2**) and Pd@ICRM(**3**).[71] The positive effect of localized amine is also supported by the literature. Mori and Yamashita, for example, showed that phenylamine-functionalized mesoporous silica helped PdAg nanoparticles in their hydrogenation of CO_2, due to the abilities of the amine to bind the substrate.[72]

The nature and the concentration of the external base (i.e., 0.7 M Et_3N) was chosen based on our screening. Figure 2 shows the TON of the CO_2 hydrogenation as a function of Et_3N/Pd ratio. Our study shows that the initial increase of amine quickly boosted the conversion but higher concentrations of the base then decreased the conversion. Similar behavior has been observed with Rh-based homogeneous catalysts.[34] In our case, the conversion was the highest at Et_3N/Pd = 250–350.

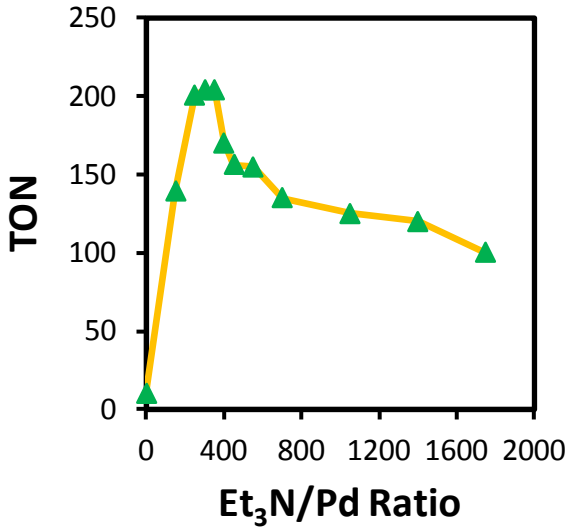

Figure 2. TON as a function of the amount of base used in the CO_2 reduction.

Et_3N was also found to give the best results when several other bases were examined, both organic and inorganic (Table 5). In general, organic amines worked better than inorganic bases such as hydroxide, carbonate, or bicarbonate. Diamines such as ethylenediamine and *N*,*N*′-dimethylethylenediamine gave very poor conversion. We suspect these chelating amines might have complexed with the Pd nanoparticle much better than any other ligands around (amino groups in the ICRM core, amide) and might have passivated the metal surface as a result. We attempted the bulky Et_2NiPr, hoping the sterically demanding nonpolar amine may prefer to reside outside the ICRM core so that the localized amines might function even better in our mechanism. Unfortunately, the yield was lower than with Et_3N as the base. We also studied the effects of localized metal oxides but found they generally lowered the TON of the Pd catalysts to 85–190 (data not shown). Apparently, reduction of CO_2 and bicarbonate had different requirements for the catalysts.

Table 5. Hydrogenation of CO_2 by Pd@ICRM(**2**) using different bases.[a]

Entry	base	TON
1	Et_3N	204
2	Bu_2NH	84
3	$HN_2CH_2CH_2NH_2$	10
4	$MeHNCH_2CH_2NHMe$	19
5	$iPrEt_2N$	147
6	KOH	<10[b]

7	$KHCO_3$	<10[b]
8	K_2CO_3	<10[b]

[a] The ICRM was prepared from surfactant **2** with Pd-loading = $[H_2PdCl_4]/[\mathbf{2}]$ = 50% and W_0 = 20. The reaction was performed in 0.2 mL THF and 0.3 mL D_2O under 40 bar H_2 and 40 bar CO_2 at 40 °C for 20 h with 0.001 mmol Pd and 0.350 mmol base. The amount of formate formed was determined by ^{1}H-NMR spectroscopy with 0.1 mmol DMF as the internal standard. [b] The reaction was performed in D_2O.

Solvents also made some difference in the CO_2 reduction. Aqueous methanol and DMSO gave very poor results. Dioxane/water mixtures, as shown in Table 6, gave somewhat better results, with TON up to 250. Interestingly, the reaction worked fairly well in water but poorly in 1,4-dioxane alone. The results agree with the literature that strong solvation of the formate by water facilitates the conversion of gaseous CO_2,[34] a generally entropically unfavorable process. When the relative ratio of H_2 and CO_2 was varied while the total pressure (= 80 bar) kept the same, the best results were obtained with a 1:1 ratio of the two (Table 6, entries 5, 8, and 9).

Table 6. Hydrogenation of CO_2 by Pd@ICRM(**2**).[a]

Entry	solvent	ratio	TON
1	THF/water	2/3	204
2	1,4-dioxane/water	0/5	217
3	1,4-dioxane/water	1/4	204
4	1,4-dioxane/water	2/3	190
5	1,4-dioxane/water	3/2	250

6	1,4-dioxane/water	4/1	250
7	1,4-dioxane/water	5/0	79
8	1,4-dioxane/water	3/2	175[b]
9	1,4-dioxane/water	3/2	182[c]

[a] The ICRM was prepared from surfactant **2** with Pd-loading = $[H_2PdCl_4]/[\mathbf{2}]$ = 50% and W_0 = 20. The reaction was performed in 0.2 mL THF and 0.3 mL D_2O under 40 bar H_2 and 40 bar CO_2 at 40 °C for 20 h with 0.001 mmol Pd and 0.350 mmol Et_3N. The amount of formate formed was determined by ^{1}H-NMR spectroscopy with 0.1 mmol DMF as the internal standard. [b] 20 bar of CO_2 and 60 bar of H_2 were used. [c] 60 bar of CO_2 and 20 bar of H_2 were used.

Conclusions

Out study shows that ICRMs are interesting organic materials for the microenvironmental engineering of entrapped catalysts through different functional groups introduced in their hydrophilic core. Their hydrophilic core not only could be used for templated synthesis of inorganic nanoparticles but also allowed localized miniature sol–gel synthesis to modify the properties of the nanoparticles. In this work, tertiary amines in the ICRM core gave significantly better results than quaternary ammonium ions in CO_2 hydrogenation, but the opposite was true in bicarbonate reduction. The catalytic reactions support the models presented in Scheme 2 and demonstrate a novel way to fine tune catalysts through environmental control. Because different functionalities can be introduced quite easily on the surfactant, their covalent capture leads to a nanospace with highly concentrated functional groups. Through this approach, it is quite likely that additional improvements can be made to enhance the catalysts' performance, in both activity[49] and selectivity.[51]

Experimental Section

General. All reagents and solvents were of ACS certified grade or higher and were used as received from commercial suppliers. Routine ^{1}H and ^{13}C NMR spectra were recorded on a Varian VXR-400 and Bruker DRX-400 spectrometer. ESI-MS was performed on a FINNIGAN TSQ700 mass spectrometer. Dynamic light scattering (DLS) was performed on a PD2000DLS^{PLUS} dynamic light scattering detector. Fluorescence spectra were recorded at ambient temperature on a Varian Cary Eclipse fluorescence spectrophotometer. UV-vis spectra were recorded at ambient temperature on a Cary 50 Bio UV-visible spectrophotometer. Syntheses of compounds **1** and **2**, as well as their ICRMs have been reported previously.[29,49]

Synthesis of Compound 3. *N,N′*-((methylazanediyl)bis(propane-3,1-diyl))diacrylamide[73] (0.75 g, 3.0 mmol) was dissolved in solution of 5-(bromomethyl)-1,2,3-tris(dodecyloxy)benzene[29] (2.5 g, 3.5 mmol) in $CHCl_3$ (30 mL). The reaction mixture was stirred at 50 °C for 36 h. The organic solvent was removed *in vacuo* and the residue was purified by column chromatography over silica gel using CH_2Cl_2 /MeOH=20/1 to 10/1 as the eluent to give a white powder (2.43 g, 72 %). ^{1}H NMR (400 MHz, $CDCl_3$, δ): 8.13 (t, *J* = 4.0 Hz, 2H), 6.59 (s, 2H), 6.46 (dd, *J* = 11.2 Hz and 6.8 Hz, 2H), 6.32 (d, *J* = 11.2 Hz, 2H), 5.64 (d, *J* = 6.8 Hz, 2H), 4.34 (s, 2H), 3.98 (t, *J* = 4.0 Hz, 6H), 3.61-3.42 (m, 8H), 2.95 (s, 3H), 2.23-2.06 (m, 4H), 1.82-1.72 (m, 6H), 1.50-1.45 (m, 6H), 1.37-1.26 (m, 48H), 0.88 (t, *J* = 4.0 Hz, 9H) ^{13}C NMR (100 MHz, $CDCl_3$, δ):166.72, 153.72, 140.51, 131.03, 126.52, 120.42, 111.16, 73.62, 69.67, 67.37, 59.11, 48.20, 35.88, 31.94, 30.37, 29.77, 29.76, 29.74, 29.71, 29.67, 29.61, 29.50, 29.41, 29.39, 26.16, 26.09, 22.70, 14.13. ; ESI-MS (*m*/*z*): $[M+H]^+$ calcd for $C_{56}H_{102}N_3O_5$, 896.7814; found 896.7819.

General procedure for the preparation of ICRM. Preparation of ICRMs and detailed characterization of the materials have been reported previously.[29,32] Typically, compound **1** (18.7 mg, 0.02 mmol) was dissolved in 0.5 ml of heptane, to which water (1.8 μL, 0.1 mmol) was added. The mixture was ultrasonicated at room temperature until the water droplet dissolved in the mixture and the solution became completely clear. After addition of 2-hydroxy-1-(4-(2-hydroxyethoxy)phenyl)-2-methylpropan-1-one (0.224 mg, 1 × 1 μmol), the mixture was irradiated in a Rayonet photoreactor for 2 h until alkenic

protons in **1** were consumed. The organic solvents were removed by rotary evaporation and the residue was washed by cold methanol and dried under vacuum to give a yellowish power (13.2 mg).

General procedure for the preparation of Pd@ICRM. Preparation of Pd@ICRMs and characterization of the materials have been reported previously.[50] An aqueous solution of H_2PdCl_4 (10 mM) was prepared by adding HCl (6 mL, 0.4 M) to $PdCl_2$ (1.2 mmol) in water (114 mL). A portion (2 mL) of the above H_2PdCl_4 solution was added to an ICRM solution in chloroform (2 mL, [**2**] = 10 mM). After stirred overnight, the mixture was allowed to sit at room temperature. The orange-colored organic phase was separated, washed with water three times, and concentrated by rotary evaporation to give an orange powder. For the UV-vis measurement, 0.1 mL of the chloroform solution was diluted by 9.9 mL of chloroform so that the concentration of the cross-linked [**2**] was 0.1 mM in the final sample.

TEM and EDX Analysis. For the TEM imaging, 5 mg of the ICRM was dissolved in 1 mL of chloroform and the solution was ultrasonicated for 1 min. A microsyringe was used to load one small drop of the above solution onto a TEM copper grid covered with carbon film. The sample was left to dry at room temperature overnight. The HAADF-STEM imaging was obtained at 200kV on a FEI Titan Themis 300 TEM with a Super-X EDX detector from the Sensitive Instrument Facility at the Ames Laboratory.

ASSOCIATED CONTENT

Supporting Information

Additional figures and NMR data for compound **2**. This material is available free of charge via the Internet at http://pubs.acs.org.

AUTHOR INFORMATION

Corresponding Author

*E-mail: zhaoy@iastate.edu

Acknowledgments

We thank NSF (CHE-1708526) for supporting this research and thank Mr. Tian Wei Goh in Prof. Wenyu Huang's group at Iowa State University for performing the TEM and EDX experiments.

Notes

The authors declare no competing financial interest.

References

(1) Das, S.; Brudvig, G. W.; Crabtree, R. H. Molecular Recognition in Homogeneous Transition Metal Catalysis: A Biomimetic Strategy for High Selectivity. *Chem. Commun.* **2008**, 413-424.

(2) Rakowski DuBois, M.; DuBois, D. L. The Roles of the First and Second Coordination Spheres in the Design of Molecular Catalysts for H_2 Production and Oxidation. *Chem. Soc. Rev.* **2009**, *38*, 62-72.

(3) Crooks, R. M.; Zhao, M. Q.; Sun, L.; Chechik, V.; Yeung, L. K. Dendrimer-Encapsulated Metal Nanoparticles: Synthesis, Characterization, and Applications to Catalysis. *Acc. Chem. Res.* **2001**, *34*, 181-190.

(4) Zhao, M.; Crooks, R. M. Homogeneous Hydrogenation Catalysis with Monodisperse, Dendrimer-Encapsulated Pd and Pt Nanoparticles. *Angew. Chem. Int. Ed.* **1999**, *38*, 364-366.

(5) Somorjai, G. A.; Li, Y. M. Selective Nanocatalysis of Organic Transformation by Metals: Concepts, Model Systems, and Instruments. *Top. Catal.* **2010**, *53*, 832-847.

(6) Chi, Y. G.; Scroggins, S. T.; Frechet, J. M. J. One-Pot Multi-Component Asymmetric Cascade Reactions Catalyzed by Soluble Star Polymers with Highly Branched Non-Interpenetrating Catalytic Cores. *J. Am. Chem. Soc.* **2008**, *130*, 6322-6323.

(7) Rodionov, V.; Gao, H.; Scroggins, S.; Unruh, D. A.; Avestro, A.-J.; Fréchet, J. M. J. Easy Access to a Family of Polymer Catalysts from Modular Star Polymers. *J. Am. Chem. Soc.* **2010**, *132*, 2570-2572.

(8) Fiedler, D.; Leung, D. H.; Bergman, R. G.; Raymond, K. N. Selective Molecular Recognition, C−H Bond Activation, and Catalysis in Nanoscale Reaction Vessels. *Acc. Chem. Res.* **2004**, *38*, 349-358.

(9) Vriezema, D. M.; Aragones, M. C.; Elemans, J.; Cornelissen, J.; Rowan, A. E.; Nolte, R. J. M. Self-Assembled Nanoreactors. *Chem. Rev.* **2005**, *105*, 1445-1489.

(10) Rebek, J. Simultaneous Encapsulation: Molecules Held at Close Range. *Angew. Chem. Int. Ed.* **2005**, *44*, 2068-2078.

(11) Yoshizawa, M.; Klosterman, J. K.; Fujita, M. Functional Molecular Flasks: New Properties and Reactions within Discrete, Self-Assembled Hosts. *Angew. Chem. Int. Ed.* **2009**, *48*, 3418-3438.

(12) Corma, A. From Microporous to Mesoporous Molecular Sieve Materials and Their Use in Catalysis. *Chem. Rev.* **1997**, *97*, 2373-2420.

(13) Huh, S.; Chen, H.-T.; Wiench, J. W.; Pruski, M.; Lin, V. S. Y. Cooperative Catalysis by General Acid and Base Bifunctionalized Mesoporous Silica Nanospheres. *Angew. Chem. Int. Ed.* **2005**, *44*, 1826-1830.

(14) Hudson, S.; Cooney, J.; Magner, E. Proteins in Mesoporous Silicates. *Angew. Chem. Int. Ed.* **2008**, *47*, 8582-8594.

(15) Thomas, J. M.; Raja, R. Exploiting Nanospace for Asymmetric Catalysis: Confinement of Immobilized, Single-Site Chiral Catalysts Enhances Enantioselectivity. *Acc. Chem. Res.* **2008**, *41*, 708-720.

(16) Ma, L.; Abney, C.; Lin, W. Enantioselective Catalysis with Homochiral Metal-Organic Frameworks. *Chem. Soc. Rev.* **2009**, *38*, 1248-1256.

(17) Corma, A.; García, H.; Llabrés i Xamena, F. X. Engineering Metal Organic Frameworks for Heterogeneous Catalysis. *Chem. Rev.* **2010**, *110*, 4606-4655.

(18) Lee, J.; Farha, O. K.; Roberts, J.; Scheidt, K. A.; Nguyen, S. T.; Hupp, J. T. Metal-Organic Framework Materials as Catalysts. *Chem. Soc. Rev.* **2009**, *38*, 1450-1459.

(19) Farrusseng, D.; Aguado, S.; Pinel, C. Metal-Organic Frameworks: Opportunities for Catalysis. *Angew. Chem. Int. Ed.* **2009**, *48*, 7502-7513.

(20) Zhou, Y. B.; Ryu, E.-H.; Zhao, Y.; Woo, L. K. Solvent-Responsive Metalloporphyrins: Binding and Catalysis. *Organometallics* **2007**, *26*, 358-364.

(21) Cho, H.; Zhong, Z.; Zhao, Y. A Dmap-Functionalized Oligocholate Foldamer for Solvent-Responsive Catalysis. *Tetrahedron* **2009**, *65*, 7311-7316.

(22) Zhang, S.; Zhao, Y. Artificial Metalloenzymes Via Encapsulation of Hydrophobic Transition-Metal Catalysts in Surface-Crosslinked Micelles (SCMs). *Chem. Commun.* **2012**, *48*, 9998-10000.

(23) Chadha, G.; Zhao, Y. Histidine-Functionalized Water-Soluble Nanoparticles for Biomimetic Nucleophilic/General-Base Catalysis under Acidic Conditions. *Org. Biomol. Chem.* **2013**, *11*, 6849-6855.

(24) Chadha, G.; Zhao, Y. Environmental Control of Nucleophilic Catalysis in Water. *Chem. Commun.* **2014**, *50*, 2718-2720.

(25) Pileni, M. P.: *Structure and Reactivity in Reverse Micelles*; Elsevier: Amsterdam, 1989.

(26) Fendler, J. H.: *Membrane Mimetic Chemistry*; Wiley: New York, 1982.

(27) Jung, H. M.; Price, K. E.; McQuade, D. T. Synthesis and Characterization of Cross-Linked Reverse Micelles. *J. Am. Chem. Soc.* **2003**, *125*, 5351-5355.

(28) Price, K. E.; McQuade, D. T. A Cross-Linked Reverse Micelle-Encapsulated Palladium Catalyst. *Chem. Commun.* **2005**, 1714-1716.

(29) Zhang, S.; Zhao, Y. Facile Preparation of Organic Nanoparticles by Interfacial Cross-Linking of Reverse Micelles and Template Synthesis of Subnanometer Au−Pt Nanoparticles. *ACS Nano* **2011**, *5*, 2637-2646.

(30) Pileni, M. P. Nanosized Particles Made in Colloidal Assemblies. *Langmuir* **1997**, *13*, 3266-3276.

(31) Pileni, M. P. The Role of Soft Colloidal Templates in Controlling the Size and Shape of Inorganic Nanocrystals. *Nat. Mater.* **2003**, *2*, 145-150.

(32) Zhang, S.; Zhao, Y. Template Synthesis of Subnanometer Gold Clusters in Interfacially Cross-Linked Reverse Micelles Mediated by Confined Counterions. *Langmuir* **2012**, *28*, 3606-3613.

(33) Jessop, P. G.; Ikariya, T.; Noyori, R. Homogeneous Hydrogenation of Carbon-Dioxide. *Chem. Rev.* **1995**, *95*, 259-272.

(34) Jessop, P. G.; Joo, F.; Tai, C. C. Recent Advances in the Homogeneous Hydrogenation of Carbon Dioxide. *Coord. Chem. Rev.* **2004**, *248*, 2425-2442.

(35) Enthaler, S.; von Langermann, J.; Schmidt, T. Carbon Dioxide and Formic Acid—The Couple for Environmental-Friendly Hydrogen Storage? *Energy Environ. Sci.* **2010**, *3*, 1207-1217.

(36) Cokoja, M.; Bruckmeier, C.; Rieger, B.; Herrmann, W. A.; Kuhn, F. E. Transformation of Carbon Dioxide with Homogeneous Transition-Metal Catalysts: A Molecular Solution to a Global Challenge? *Angew. Chem. Int. Ed.* **2011**, *50*, 8510-8537.

(37) Wang, W.; Wang, S.; Ma, X.; Gong, J. Recent Advances in Catalytic Hydrogenation of Carbon Dioxide. *Chem. Soc. Rev.* **2011**, *40*, 3703-3727.

(38) Appel, A. M.; Bercaw, J. E.; Bocarsly, A. B.; Dobbek, H.; DuBois, D. L.; Dupuis, M.; Ferry, J. G.; Fujita, E.; Hille, R.; Kenis, P. J.; Kerfeld, C. A.; Morris, R. H.; Peden, C. H.; Portis, A. R.; Ragsdale, S. W.; Rauchfuss, T. B.; Reek, J. N.; Seefeldt, L. C.; Thauer, R. K.; Waldrop, G. L. Frontiers, Opportunities, and Challenges in Biochemical and Chemical Catalysis of CO_2 Fixation. *Chem. Rev.* **2013**, *113*, 6621-6658.

(39) Wang, W. H.; Himeda, Y.; Muckerman, J. T.; Manbeck, G. F.; Fujita, E. CO_2 Hydrogenation to Formate and Methanol as an Alternative to Photo- and Electrochemical CO_2 Reduction. *Chem. Rev.* **2015**, *115*, 12936-12973.

(40) Stalder, C. J.; Chao, S.; Summers, D. P.; Wrighton, M. S. Supported Palladium Catalysts for the Reduction of Sodium-Bicarbonate to Sodium Formate in Aqueous-Solution at Room-Temperature and One Atmosphere of Hydrogen. *J. Am. Chem. Soc.* **1983**, *105*, 6318-6320.

(41) Wiener, H.; Blum, J.; Feilchenfeld, H.; Sasson, Y.; Zalmanov, N. The Heterogeneous Catalytic-Hydrogenation of Bicarbonate to Formate in Aqueous-Solutions. *J. Catal.* **1988**, *110*, 184-190.

(42) Gunasekar, G. H.; Park, K.; Jung, K. D.; Yoon, S. Recent Developments in the Catalytic Hydrogenation of CO_2 to Formic Acid/Formate Using Heterogeneous Catalysts. *Inorg. Chem. Front.* **2016**, *3*, 882-895.

(43) Su, J.; Yang, L. S.; Lu, M.; Lin, H. F. Highly Efficient Hydrogen Storage System Based on Ammonium Bicarbonate/Formate Redox Equilibrium over Palladium Nanocatalysts. *Chemsuschem* **2015**, *8*, 813-816.

(44) Nguyen, L. T. M.; Park, H.; Banu, M.; Kim, J. Y.; Youn, D. H.; Magesh, G.; Kim, W. Y.; Lee, J. S. Catalytic Co_2 Hydrogenation to Formic Acid over Carbon Nanotube-Graphene Supported Pdni Alloy Catalysts. *RSC Adv.* **2015**, *5*, 105560-105566.

(45) Park, H.; Lee, J. H.; Kim, E. H.; Kim, K. Y.; Choi, Y. H.; Youn, D. H.; Lee, J. S. A Highly Active and Stable Palladium Catalyst on a g-C_3N_4 Support for Direct Formic Acid Synthesis under Neutral Conditions. *Chem. Commun.* **2016**, *52*, 14302-14305.

(46) Su, J.; Lu, M.; Lin, H. High Yield Production of Formate by Hydrogenating Co_2 Derived Ammonium Carbamate/Carbonate at Room Temperature. *Green Chem.* **2015**, *17*, 2769-2773.

(47) Bi, Q. Y.; Lin, J. D.; Liu, Y. M.; Du, X. L.; Wang, J. Q.; He, H. Y.; Cao, Y. An Aqueous Rechargeable Formate-Based Hydrogen Battery Driven by Heterogeneous Pd Catalysis. *Angew. Chem. Int. Ed.* **2014**, *53*, 13583-13587.

(48) Israelachvili, J. N.: *Intermolecular and Surface Forces: With Applications to Colloidal and Biological Systems*; Academic Press: London, 1985.

(49) Lee, L.-C.; Zhao, Y. Metalloenzyme-Mimicking Supramolecular Catalyst for Highly Active and Selective Intramolecular Alkyne Carboxylation. *J. Am. Chem. Soc.* **2014**, *136*, 5579-5582.

(50) Lee, L.-C.; Zhao, Y. Interfacially Cross-Linked Reverse Micelles as Soluble Support for Palladium Nanoparticle Catalysts. *Helv. Chim. Acta* **2012**, *95*, 863-871.

(51) Lee, L.-C.; Zhao, Y. Size-Selective Phase-Transfer Catalysis with Interfacially Cross-Linked Reverse Micelles. *Org. Lett.* **2012**, *14*, 784-787.

(52) Lee, L. C.; Xiao, C. X.; Huang, W. Y.; Zhao, Y. Palladium-Gold Bimetallic Nanoparticle Catalysts Prepared by "Controlled Release" from Metal-Loaded Interfacially Cross-Linked Reverse Micelles. *New. J. Chem.* **2015**, *39*, 2459-2466.

(53) Allam, R. J.; Bredesen, R.; Drioli, E.: In *Carbon Dioxide Recovery and Utilization*; Aresta, M., Ed.; Kluwer Academic Publisher, 2003; pp 53-118.

(54) Yoshio, I.; Hitoshi, I.; Yoshiyuki, S.; Harukichi, H. Catalytic Fixation of Carbon Dioxide to Formic Acid by Transition-Metal Complexes under Mild Conditions. *Chem. Lett.* **1976**, *5*, 863-864.

(55) Jessop, P. G.; Hsiao, Y.; Ikariya, T.; Noyori, R. Homogeneous Catalysis in Supercritical Fluids: Hydrogenation of Supercritical Carbon Dioxide to Formic Acid, Alkyl Formates, and Formamides. *J. Am. Chem. Soc.* **1996**, *118*, 344-355.

(56) Joo, F.; Joo, F.; Nadasdi, L.; Elek, J.; Laurenczy, G.; Nadasdi, L. Homogeneous Hydrogenation of Aqueous Hydrogen Carbonate to Formate under Exceedingly Mild Conditions-a Novel Possibility of Carbon Dioxide Activation[Dagger]. *Chem. Commun.* **1999**, 971-972.

(57) Ziebart, C.; Federsel, C.; Anbarasan, P.; Jackstell, R.; Baumann, W.; Spannenberg, A.; Beller, M. Well-Defined Iron Catalyst for Improved Hydrogenation of Carbon Dioxide and Bicarbonate. *J. Am. Chem. Soc.* **2012**, *134*, 20701-20704.

(58) Jeletic, M. S.; Mock, M. T.; Appel, A. M.; Linehan, J. C. A Cobalt-Based Catalyst for the Hydrogenation of CO_2 under Ambient Conditions. *J. Am. Chem. Soc.* **2013**, *135*, 11533-11536.

(59) Hull, J. F.; Himeda, Y.; Wang, W.-H.; Hashiguchi, B.; Periana, R.; Szalda, D. J.; Muckerman, J. T.; Fujita, E. Reversible Hydrogen Storage Using CO_2 and a Proton-Switchable Iridium Catalyst in Aqueous Media under Mild Temperatures and Pressures. *Nat. Chem.* **2012**, *4*, 383-388.

(60) Tanaka, R.; Yamashita, M.; Nozaki, K. Catalytic Hydrogenation of Carbon Dioxide Using Ir(III)−Pincer Complexes. *J. Am. Chem. Soc.* **2009**, *131*, 14168-14169.

(61) Balaraman, E.; Gunanathan, C.; Zhang, J.; Shimon, L. J. W.; Milstein, D. Efficient Hydrogenation of Organic Carbonates, Carbamates and Formates Indicates Alternative Routes to Methanol Based on Co2 and Co. *Nat. Chem.* **2011**, *3*, 609-614.

(62) Huff, C. A.; Sanford, M. S. Cascade Catalysis for the Homogeneous Hydrogenation of Co2 to Methanol. *J. Am. Chem. Soc.* **2011**, *133*, 18122-18125.

(63) Rezayee, N. M.; Huff, C. A.; Sanford, M. S. Tandem Amine and Ruthenium-Catalyzed Hydrogenation of CO_2 to Methanol. *J. Am. Chem. Soc.* **2015**, *137*, 1028-1031.

(64) *Nanoparticles and Catalysis*; Astruc, D., Ed.; Wiley-VCH: Weinheim, Germany, 2008.

(65) Bell, A. T. The Impact of Nanoscience on Heterogeneous Catalysis. *Science* **2003**, *299*, 1688-1691.

(66) Somorjai, G. A.; Contreras, A. M.; Montano, M.; Rioux, R. M. Clusters, Surfaces, and Catalysis. *Proc. Natl. Acad. Sci. U. S. A.* **2006**, *103*, 10577-10583.

(67) Burda, C.; Chen, X.; Narayanan, R.; El-Sayed, M. A. Chemistry and Properties of Nanocrystals of Different Shapes. *Chem. Rev.* **2005**, *105*, 1025-1102.

(68) Lee, L.-C.; Zhao, Y. Room Temperature Hydroamination of Alkynes Catalyzed by Gold Clusters in Interfacially Cross-Linked Reverse Micelles. *Acs Catal* **2014**, 688-691.

(69) Zhao, Y.; Zhong, Z.; Ryu, E.-H. Preferential Solvation within Hydrophilic Nanocavities and Its Effect on the Folding of Cholate Foldamers. *J. Am. Chem. Soc.* **2007**, *129*, 218-225.

(70) Cho, H.; Zhao, Y. Environmental Effects Dominate the Folding of Oligocholates in Solution, Surfactant Micelles, and Lipid Membranes. *J. Am. Chem. Soc.* **2010**, *132*, 9890-9899.

(71) It would be ideal if the formation of carbamate with the localized amines in the ICRM core could be detected spectroscopically. However, our reaction mixture contained a large amount of triethylamine, which could also form carbamate reversibly with CO_2 by the same mechanism. Therefore, even if the formation of carbamate could be detected under the high pressure condition, most of the carbamate should come from the background, i.e., reaction with triethylamine.

(72) Mori, K.; Masuda, S.; Tanaka, H.; Yoshizawa, K.; Che, M.; Yamashita, H. Phenylamine-Functionalized Mesoporous Silica Supported Pdag Nanoparticles: A Dual Heterogeneous Catalyst for Formic Acid/ CO_2-Mediated Chemical Hydrogen Delivery/Storage. *Chem. Commun.* **2017**, *53*, 4677-4680.

(73) Lee, L.-C.; He, J.; Yu, J.-Q.; Jones, C. W. Functionalized Polymer-Supported Pyridine Ligands for Palladium-Catalyzed C(sp^3)–H Arylation. *Acs Catal* **2016**, *6*, 5245-5250.

TOC graphic